Effective bond-orbital model for shallow acceptors in GaAs-$Al_xGa_{1-x}As$ quantum wells and superlattices

G. T. Einevoll
Department of Physics and Materials Research Laboratory, University of Illinois at Urbana-Champaign, Urbana, Illinois 61801 and Institutt for Fysikk, Norges Tekniske Høgskole, Universitetet i Trondheim, N-7034 Trondheim NTH, Norway

Yia-Chung Chang
Department of Physics and Materials Research Laboratory, University of Illinois at Urbana-Champaign, Urbana, Illinois 61801
(Received 3 August 1989)

The novel effective bond-orbital model (EBOM) is used to calculate energies of shallow acceptors in GaAs-$Al_xGa_{1-x}As$ quantum wells and superlattices. The model is tight-binding-like, and the interactions between bond orbitals located at sites in the face-centered-cubic lattice are fitted to make EBOM predict the right band structure close to the valence-band edge. Symmetry-adapted functions consisting of proper linear combinations of bond orbitals located at sites in the vicinity of the acceptor impurity are used as basis functions in variational calculations of energies of acceptor states. First, we calculate energies of both Γ_6 (heavy-hole) and Γ_7 (light-hole) ground states and first even-parity excited states for C and Be acceptors centered in the well material of single quantum wells. When comparing EBOM results with results from previous multiband effective-mass calculations, we generally find good agreement for the ground-state energies and the corresponding binding energies, while the estimates for the excited states vary substantially. Comparisons with recent experiments, where two independent experimental techniques are used to measure energies of transitions involving the excited states, favor the EBOM results. The deviations of the effective-mass results are thought to reflect inherent shortcomings in the effective-mass method, absent in the EBOM, namely the calculational difficulty of properly incorporating position-dependent material parameters and the practical limitations on the flexibility of trial wave functions in actual calculations. Finally, the EBOM is used to calculate binding energies of acceptors in superlattices. Up to 11 wells are included in the model for the thinnest superlattices in which coupling of adjacent wells is essential. In order to compare with recent photoluminescence experiments on C acceptors in narrow-barrier superlattices, the corresponding EBOM calculations for both well- and barrier-centered acceptors in superlattices are performed.

I. INTRODUCTION

The recent advances in crystal-growth techniques such as molecular-beam epitaxy (MBE) and metalorganic chemical vapor deposition (MOCVD) have triggered extensive studies on artificial superlattices and quantum wells. The ability of controlling material composition and intentionally incorporating impurities on the atomic scale has led to numerous experimental studies of electronic energy levels for shallow impurities embedded in heterostructures. These measurements, which include photoluminescence,[1-5] Raman scattering,[4,6,7] magnetospectroscopy,[5,8] and far-infrared absorption,[9] have so far mainly focused on impurities in GaAs-$Al_xGa_{1-x}As$ systems.

All previous theoretical calculations have been within the framework of effective-mass theory. In a pioneering paper Bastard[10] calculated energies of donor states in quantum wells assuming infinite barrier height. The binding energy, defined as the difference between the ground-state energies with and without a donor centered in the well, was found to increase monotonically with decreasing well width. In more realistic calculations which included finite barrier heights, the binding energy was found to have a maximum at a finite well width.[11,12] For the well width corresponding to the maximum, the confinement energy for the pure quantum well is substantial, while the impurity, to a large extent, manages to localize the wave function within the well material. As the well width approaches zero, the impurity wave function leaks more and more into the barrier, and the binding energy will eventually go to the bulk value for the barrier material.

Acceptor calculations are generally more difficult due to the complicated valence bands. Masselink *et al.*[13] calculated the energy spectra for acceptors in GaAs-$Al_xGa_{1-x}As$ quantum wells with finite barrier heights, taking the top four valence bands of both the well and barrier material into account. The resulting binding energies showed the same characteristic dependence on well width and were also found to be in good agreement with available experimental data.

In practice, quantum-well measurements are done on GaAs-$Al_xGa_{1-x}As$ superlattices with sufficiently high and wide barriers to avoid coupling between adjacent wells. For superlattices involving low (i.e., small fraction of aluminum in the barrier alloy) or narrow barriers, interwell coupling may be substantial and cannot be

neglected in calculations. To allow for interwell coupling, Chaudhuri[14] included the two neighboring wells in a calculation of donor energies. Setting the barrier width and well width equal, the binding energy as a function of well width was found to have two maxima. The primary peak was found to be shifted towards larger well widths compared to the binding-energy curve for single quantum wells. The secondary peak, corresponding to very narrow wells and barriers, was attributed to the breakdown of the approximation of including only three wells in a model for short-period superlattices.

While effective-mass theory is on a solid footing for impurities in bulk semiconductors,[15] the extension of the theory to heterostructures is nontrivial, with complications arising from the position-dependent material parameters. The theory is not asymptotically exact in the limit of infinitely shallow impurity potential for heterostructures with nonzero offsets (i.e., band edges are not aligned),[16] but this does not exclude the possibility that effective-mass theory may give good results. For donor problems, where one-band effective-mass theory is appropriate, the boundary conditions for the matching of envelope functions at abrupt material interfaces seem to be well established.[16–21] Boundary conditions based on continuity of probability current have been worked out for degenerate-band effective-mass theory ($\mathbf{k}\cdot\mathbf{p}$),[22] but they are complicated and hard to include in acceptor calculations. To our knowledge, no calculations on acceptors in heterostructures which take into account the full valence-band degeneracy and match the envelope functions at the interfaces have been done. In fact, most reported calculations on the much simpler donor problems have been on models where the position dependence of material parameters is ignored or treated in an approximate way. So, even in the cases where proper effective-mass treatment, in principle, gives good results for impurities in heterostructures, the complicated implementation of the method severely reduces its feasibility.

In this article we use the novel effective bond-orbital model (EBOM) to calculate energies for acceptors in quantum wells and superlattices. Harrison[23] introduced the bond-orbital model to describe properties of covalent and polar solids and obtained the interaction parameters using atomic properties and the value of the static dielectric constant. The model was reformulated by Chang[24] to be used in calculations on electronic states involving small wave numbers in semiconductors and semiconductor heterostructures. Instead of trying to estimate the interaction parameters from microscopic considerations, these parameters were fitted to predict the experimentally observed bulk band structure close to the Brillouin zone center. The first applications of the method were in calculations of superlattice band structures for both large–band-gap and small–band-gap heterostructures.[24,25]

In a recent paper[26] the authors introduced the model as a new framework for calculating properties of localized states and used the method to calculate energies for acceptors in bulk semiconductors and acceptors embedded in GaAs-$Al_xGa_{1-x}As$ spherical quantum dots. The term *effective bond-orbital model* was introduced to avoid confusion with Harrison's version and to stress that the *real* bond orbitals are not expected to interact like these *effective* bond orbitals. The usefulness of the effective bond orbitals lies in their ability to describe both extended and localized electronic states with wave functions with slowly varying envelopes.

The EBOM may be viewed as a discretized version of the effective-mass theory with the grid spacing given by the lattice constant. In the EBOM the positional dependence of material parameters is straightforward to include in the calculation, and this feature makes the method more applicable to problems involving impurities in heterostructures than effective-mass theory.

In Sec. II we first quickly review the EBOM formalism before we show how group theory is utilized to obtain an appropriate set of basis functions suitable for variational calculations. The group-theory treatment is similar to the treatment in Ref. 26 for acceptors in bulk semiconductors and spherical quantum dots, but the presence of a quantum well (or superlattice) has lowered the symmetry of the problem. At the end of the section a very useful scaling approximation which reduces the computer time needed in the calculations is described. In Sec. III we apply the method to acceptors located at the center of single GaAs-$Al_{0.3}Ga_{0.7}As$ quantum wells. Ground-state energies, corresponding binding energies, and energies of even-parity excited states are calculated and compared with experiments and previous multiband effective-mass calculations. In Sec. IV we first study acceptors in short-period GaAs-$Al_{0.3}Ga_{0.7}As$ superlattices where coupling between adjacent wells become important, including up to 11 wells in the calculations. Comparison of qualitative features of energy spectra with previous donor calculations are made. In order to compare with recent photoluminescence experiments by Skromme *et al.*,[3,27] where coupling of wells is important, we also perform calculations of binding energies for acceptors centered in the barrier and well material, respectively, for a set of superlattices with compositions according to the samples used in the measurements.

II. THEORY

This section is divided into three subsections. In the first subsection we swiftly describe the bond-orbital formalism and provide the formulas for the interactions needed in the calculations. For more details, we refer to Refs. 24 and 26. In the second subsection we utilize the theory of point groups to construct basis functions to be used in variational calculations. A scaling approximation is described in the last subsection. For more discussion on this approximation, we refer to Ref. 26.

A. Bond orbitals

Diamond– and zinc-blende–structure crystals consist of a unit cell containing two atoms located at the sites of the face-centered-cubic (fcc) lattice. For acceptors in large-gap band-semiconductors or heterostructures made of large-gap band-materials, a bond-orbital model which includes only the topmost valence bands is sufficient. A bond orbital is, in this context, defined as the proper

linear combination of atomic orbitals in a unit cell which best describes the experimentally observed band structure close to the zone center. If spin-orbit coupling is negligible, the bond orbitals are p-like (labeled x,y,z). They are assumed to be sufficiently localized so that only on-site and nearest-neighbor interactions have to be considered. We use the notation $|\mathbf{R},\alpha\rangle$ for an α-like ($\alpha=x,y,z$) bond orbital located at lattice site $\mathbf{R}$. The general form of the interactions between two bond orbitals is known from symmetry considerations to be[28]

$$\langle \mathbf{R},\alpha|H|\mathbf{R}',\alpha'\rangle = E_p\delta_{\mathbf{R},\mathbf{R}'}\delta_{\alpha,\alpha'} + \sum_{\tau}\delta_{\mathbf{R}'-\mathbf{R},\tau}\{E_{xy}\tau_\alpha\tau_{\alpha'}(1-\delta_{\alpha,\alpha'}) + [E_{xx}\tau_\alpha^2 + E_{zz}(1-\tau_\alpha^2)]\delta_{\alpha,\alpha'}\} \ . \tag{1}$$

$E_{\alpha,\alpha'}$ denotes the interaction between an α-like orbital at the origin and an α'-like orbital at $(1,1,0)a/2$. E_p, E_{xx}, E_{xy}, and E_{zz} are four independent interaction parameters, and the sum over τ covers the 12 nearest-neighbor position vectors. τ_α denotes the α component of τ in units of $a/2$.

With a non-negligible spin-orbit coupling present, which certainly is the case for GaAs-$Al_xGa_{1-x}As$ systems, the spin-orbit-coupled bond orbitals (SOBO's) represent a more practical basis. In the angular-momentum convention the SOBO's have the form

$$|\mathbf{R},u_M^J\rangle = \sum_{\alpha,\sigma} C(\alpha,\sigma;J,M)|\mathbf{R},\alpha\rangle\chi_\sigma \ , \tag{2}$$

where $J=\frac{3}{2},\frac{1}{2}$, $M=-J,-J+1,\ldots,J$, and χ_σ, $\sigma=\frac{1}{2},-\frac{1}{2}$, denotes the electron spinors. The coupling coefficients $C(\alpha,\sigma;J,M)$ are known from group theory and can be found, e.g., in Ref. 26. With the spin-orbit coupling included, the interaction between two SOBO's is given by

$$\langle \mathbf{R},u_M^J|H|\mathbf{R}',u_{M'}^{J'}\rangle = (J-\tfrac{3}{2})\Delta\delta_{JM,J'M'}\delta_{\mathbf{R},\mathbf{R}'} + \sum_{\alpha,\alpha',\sigma} C^*(\alpha,\sigma;J,M)C(\alpha',\sigma;J',M')\langle \mathbf{R},\alpha|H|\mathbf{R}',\alpha'\rangle \ , \tag{3}$$

where Δ is the spin-orbit splitting.

The interaction parameters in Eq. (1) are determined by doing a Taylor expansion of the tight-binding Hamiltonian in the SOBO basis to second order in $\mathbf{k}$ and requiring equivalence with the effective-mass ($\mathbf{k}\cdot\mathbf{p}$) Hamiltonian.[15] A one-to-one correspondence between the Luttinger parameters[29] and the interaction parameters is thus established, namely

$$\begin{aligned} E_{xy} &= 6\gamma_3 R_0 \ , \\ E_{xx} &= (\gamma_1+4\gamma_2)R_0 \ , \\ E_{zz} &= (\gamma_1-8\gamma_2)R_0 \ , \\ E_p &= E_v - 12\gamma_1 R_0 \ . \end{aligned} \tag{4}$$

E_v refers to the band edge of the heavy- and light-hole bands and $R_0 \equiv \hbar^2/2ma^2$, where m is the free-electron mass.

The contribution to the interaction from a shallow impurity located at the origin is taken to be

$$\left\langle \mathbf{R},u_M^J \left| \frac{-e^2}{\epsilon_0 r} \right| \mathbf{R}',u_{M'}^{J'} \right\rangle = \frac{-e^2}{\epsilon_0|\mathbf{R}|}\delta_{JM,J'M'}\delta_{\mathbf{R},\mathbf{R}'}, \quad |\mathbf{R}|\neq 0 \tag{5}$$

where $-e^2/\epsilon_0 r$ is a screened Coulomb interaction. The impurity interaction between two identical SOBO's *on* the impurity site, U_0, is treated as an empirical fitting parameter. A recent report[30] has indicated that the effect of spatially dependent screening, where ϵ is a function of the distance from the impurity, cannot be neglected in effective-mass calculations for acceptors in GaAs-$Al_xGa_{1-x}As$ quantum wells. In the EBOM, however, the effect will be absorbed in the parameter U_0, and we use the static value for the dielectric screening ϵ_0 in Eq. (5).

In the application of the EBOM to heterostructures, we take interactions between any two bond orbitals located in the same material to be the same as the bulk values. For two bond orbitals in different materials, i.e., on each side of an interface, we take the interaction to be the average of the interaction in each material. For the static dielectric screening in Eq. (5), we use the bulk values for ϵ_0, which are different in the well and barrier material, and neglect image-force effects due to abrupt changes in ϵ_0 at material interfaces.[31]

We choose the z direction to be the confining direction, i.e., normal to the quantum-well or superlattice interfaces. When discussing acceptor states, it is practical to use the hole picture, and throughout this paper we use this convention. The energy scale is inverted, with the zero of energy chosen to be at the bottom (in the hole picture) of the bulk valence bands of the well material, and the interactions between holelike SOBO's correspond to the electron interactions listed in Eq. (4) multiplied by -1.

B. Basis functions

Bulk GaAs has the symmetry of the tetrahedral point group T_d. In T_d the p-like valence-band states transform like Γ_5 and the $s=\frac{1}{2}$ spinor like Γ_6, and group theory

gives that $\Gamma_5\times\Gamma_6=\Gamma_7+\Gamma_8$. An acceptor in bulk GaAs will thus give rise to two series of bound states, a Γ_7 series associated with the twofold-degenerate split-off band and a Γ_8 series associated with the heavy- or light-hole bands which are fourfold degenerate at $\mathbf{k}=0$.

The presence of a quantum well (or a periodic superlattice) reduces the symmetry from T_d to D_{2d}. In D_{2d} the p-like valence-band states transform like the Γ_4 and Γ_5 representations, while the $s=\frac{1}{2}$ spinor still transforms like Γ_6. Group theory gives $(\Gamma_4+\Gamma_5)\times\Gamma_6=\Gamma_6+{}^1\Gamma_7+{}^2\Gamma_7$. We use the Koster-Dimmock-Wheeler-Statz (KDWS) convention (u_ν^Γ) in Ref. 32, which is different from the angular-momentum convention (u_M^J) used in the preceding subsection. To stress the difference, we label the $s=\frac{1}{2}$ spinors ϕ^{Γ_6} instead of χ. In the KDWS convention we have the following SOBO's:

$$
\begin{aligned}
|\mathbf{R},u^{\Gamma_6}_{1/2}\rangle&=\frac{i}{\sqrt{2}}|\mathbf{R},x\rangle\phi^{\Gamma_6}_{-1/2}+\frac{1}{\sqrt{2}}|\mathbf{R},y\rangle\phi^{\Gamma_6}_{-1/2}\,,\\
|\mathbf{R},u^{\Gamma_6}_{-1/2}\rangle&=\frac{i}{\sqrt{2}}|\mathbf{R},x\rangle\phi^{\Gamma_6}_{1/2}-\frac{1}{\sqrt{2}}|\mathbf{R},y\rangle\phi^{\Gamma_6}_{1/2}\,,
\end{aligned}
\tag{6}
$$

and

$$
\begin{aligned}
|\mathbf{R},{}^1u^{\Gamma_7}_{1/2}\rangle&=-i|\mathbf{R},z\rangle\phi^{\Gamma_6}_{1/2}\,,\\
|\mathbf{R},{}^1u^{\Gamma_7}_{-1/2}\rangle&=i|\mathbf{R},z\rangle\phi^{\Gamma_6}_{-1/2}\,,\\
|\mathbf{R},{}^2u^{\Gamma_7}_{1/2}\rangle&=\frac{i}{\sqrt{2}}|\mathbf{R},x\rangle\phi^{\Gamma_6}_{-1/2}-\frac{1}{\sqrt{2}}|\mathbf{R},y\rangle\phi^{\Gamma_6}_{-1/2}\,,\\
|\mathbf{R},{}^2u^{\Gamma_7}_{-1/2}\rangle&=\frac{i}{\sqrt{2}}|\mathbf{R},x\rangle\phi^{\Gamma_6}_{1/2}+\frac{1}{\sqrt{2}}|\mathbf{R},y\rangle\phi^{\Gamma_6}_{1/2}\,.
\end{aligned}
\tag{7}
$$

The large spin-orbit coupling of GaAs and $Al_xGa_{1-x}As$ alloys suggests the replacement of the above Γ_7 SOBO's by two new sets of Γ_7 SOBO's, namely

$$
\begin{aligned}
|\mathbf{R},u^{\Gamma_7}_{1/2}\rangle&=-\frac{i}{\sqrt{6}}|\mathbf{R},x\rangle\phi^{\Gamma_6}_{-1/2}+\frac{1}{\sqrt{6}}|\mathbf{R},y\rangle\phi^{\Gamma_6}_{-1/2}\\
&\quad+i\frac{2}{\sqrt{6}}|\mathbf{R},z\rangle\phi^{\Gamma_6}_{1/2}\,,\\
|\mathbf{R},u^{\Gamma_7}_{-1/2}\rangle&=\frac{i}{\sqrt{6}}|\mathbf{R},x\rangle\phi^{\Gamma_6}_{1/2}+\frac{1}{\sqrt{6}}|\mathbf{R},y\rangle\phi^{\Gamma_6}_{1/2}\\
&\quad+i\frac{2}{\sqrt{6}}|\mathbf{R},z\rangle\phi^{\Gamma_6}_{-1/2}\,,
\end{aligned}
\tag{8}
$$

and

$$
\begin{aligned}
|\mathbf{R},{}^{\text{s.o.}}u^{\Gamma_7}_{1/2}\rangle&=-\frac{i}{\sqrt{3}}|\mathbf{R},x\rangle\phi^{\Gamma_6}_{-1/2}+\frac{1}{\sqrt{3}}|\mathbf{R},y\rangle\phi^{\Gamma_6}_{-1/2}\\
&\quad-\frac{i}{\sqrt{3}}|\mathbf{R},z\rangle\phi^{\Gamma_6}_{1/2}\,,\\
|\mathbf{R},{}^{\text{s.o.}}u^{\Gamma_7}_{-1/2}\rangle&=-\frac{i}{\sqrt{3}}|\mathbf{R},x\rangle\phi^{\Gamma_6}_{1/2}-\frac{1}{\sqrt{3}}|\mathbf{R},y\rangle\phi^{\Gamma_6}_{1/2}\\
&\quad+\frac{i}{\sqrt{3}}|\mathbf{R},z\rangle\phi^{\Gamma_6}_{-1/2}\,.
\end{aligned}
\tag{9}
$$

The spin-orbit coupling lifts the energies of the Γ_7 SOBO's in Eq. (9) with Δ compared to the Γ_6 SOBO's in Eq. (6) and the Γ_7 SOBO's in Eq. (8). For GaAs-$Al_xGa_{1-x}As$ systems where Δ is $\sim$0.3 eV, it is a good approximation to assume that $|\mathbf{R},{}^{\text{s.o.}}u^{\Gamma_7}_{1/2}\rangle$ and $|\mathbf{R},{}^{\text{s.o.}}u^{\Gamma_7}_{-1/2}\rangle$ in Eq. (9) are decoupled from the rest, and we will neglect them in the present calculations. The Γ_6 SOBO's are equivalent to heavy-hole SOBO's ($J=\frac{3}{2}$, $M=\frac{3}{2},-\frac{3}{2}$) in bulk (see, e.g., Ref. 26), and states with this symmetry are thus often said to be heavy-hole-like. Correspondingly, the Γ_7 SOBO's in Eq. (8) are equivalent to light-hole SOBO's ($J=\frac{3}{2}$, $M=\frac{1}{2},-\frac{1}{2}$) in bulk and are said to be light-hole-like.

Energy eigenvalues and corresponding wave functions for acceptor states can now, in principle, be found by expanding the wave function as a linear combination of holelike SOBO's of the form in Eqs. (6) and (8) located at sites on the fcc lattice in the vicinity of the impurity, i.e., $|\psi\rangle=\sum_i C_i|\psi_i\rangle=\sum_i C_i|\mathbf{R}(i),u_\nu^\Gamma(i)\rangle$. Using the standard variational method, we obtain a set of coupled linear algebraic equations,

$$
\sum_i\left(\langle\psi_{i'}|H|\psi_i\rangle+\langle\psi_{i'}|U|\psi_i\rangle-E\langle\psi_{i'}|\psi_i\rangle\right)C_i=0\,,
\tag{10}
$$

where H represents the unperturbed Hamiltonian and U represents the impurity potential. The matrix elements in the generalized eigenvalue problem in Eq. (10) are given by Eqs. (1), (4)–(6), and (8). The numerical values for the interaction parameters in Eq. (4) naturally depend on wherein the heterostructure the bond orbitals are located. The dimension of the matrices in Eq. (10) is governed by the number of sites necessary to include in the calculations, which, in turn, depends on the spatial extension of the wave function for the acceptor state. For shallow acceptor impurities, where effective Bohr radii in bulk semiconductors are typically 20–50 Å, the required number of sites in the cluster implies matrix sizes in the generalized eigenvalue problem which drastically exceed the capacity of present-day computers. The task is therefore to find a smaller, but sufficient, set of basis functions to be used in the variational calculations, and this is most easily done utilizing the theory of point groups.

In the EBOM calculations for acceptors in bulk semiconductors and spherical quantum dots,[26] the sites in the cluster was grouped into *shells* consisting of sites connected by the symmetry operations in T_d. Projection operators were then used to generate coefficients for sites in a shell representing desired spatial symmetries, and these sets of coefficients were then coupled to SOBO's to give the desired total symmetry, namely the symmetry of the acceptor states. By using these composite functions, called *shell functions,* in the basis, a reduction of the number of basis functions by a factor 12 was achieved compared to the naive method of letting each SOBO be a separate basis function. Even with this reduction, however, the number of shell functions needed in the basis was too high, and cubic harmonics[33] were introduced as an approximation. In the actual calculations sites close to the impurity were represented by independent shell functions, while cubic harmonics multiplied with radial exponentials were used as basis functions for the long-range part of the acceptor wave functions. It turned out that while inclusion of independent shell functions in the basis

may be important for acceptors in bulk Si, they can, as a good approximation, be left out of the basis for acceptors in bulk GaAs.

The presence of a spherically symmetric impurity potential due to an acceptor centered in the well material (or barrier material in superlattices) does not change the point group of the model. Centered acceptors will thus give rise to both Γ_6- and Γ_7-like bound states. A conceivable procedure would therefore be to construct shell functions with the appropriate Γ_6 and Γ_7 symmetries to use as basis functions. The construction of these shell functions in D_{2d} follows the recipe outlined for T_d in Ref. 26. Since we are dealing with acceptors in GaAs-$Al_xGa_{1-x}As$ systems, however, *no* independent shell functions will be included in the basis. Note also that since D_{2d} contains only one-third of the elements in T_d, the benefits from using shell functions instead of separate SOBO's will be correspondingly smaller.

The EBOM introduces an artificially high symmetry by ignoring the structure within the unit cell and corresponds to the larger point group D_{4h}. D_{4h} contains inversion, and parity is a good quantum number. We prefer to use the notation of D_{2d} in the group-theory discussion below and add labeling for the parity of the state afterwards. To be consistent with the notation used in, for example, previous effective-mass calculations, we label the states by the parity of the envelope function.

In this article we focus on acceptor states with even-parity envelopes (e.g., ground states). As an approximation we include only *s*- and *d*-like angular functions in the construction of the set of basis functions.[13,26] The spherically symmetric *s*-like envelope is trivial, but the *d*-like contributions are more complicated since a *d* state splits into $\Gamma_1+\Gamma_3+\Gamma_4+\Gamma_5$ in the group D_{2d}.

We first consider the twofold-degenerate Γ_6^+ acceptor states (the label + stands for even-parity envelopes). The $\Gamma_6^{1/2}$ and $\Gamma_6^{-1/2}$ series are equivalent, and we choose to focus on states with $\Gamma_6^{1/2}$ symmetry. By considering the appropriate product of SOBO symmetries and envelope symmetries $(\Gamma_6+\Gamma_7)\times(\Gamma_1+\Gamma_3+\Gamma_4+\Gamma_5)$, using the tables in Ref. 32, we find six distinct angular functions, namely

$$
\begin{aligned}
|\psi_{1/2}^{\Gamma_6^+}(\mathbf{R})\rangle_a &= |\mathbf{R},u_{1/2}^{\Gamma_6}\rangle \ , \\
|\psi_{1/2}^{\Gamma_6^+}(\mathbf{R})\rangle_b &= \frac{Z^2-\frac{1}{2}(X^2+Y^2)}{\mathcal{R}^2}|\mathbf{R},u_{1/2}^{\Gamma_6}\rangle \ , \\
|\psi_{1/2}^{\Gamma_6^+}(\mathbf{R})\rangle_c &= \frac{\sqrt{3}}{2}\frac{X^2-Y^2}{\mathcal{R}^2}|\mathbf{R},u_{1/2}^{\Gamma_7}\rangle \ , \\
|\psi_{1/2}^{\Gamma_6^+}(\mathbf{R})\rangle_d &= -i\frac{XY}{\mathcal{R}^2}|\mathbf{R},u_{1/2}^{\Gamma_7}\rangle \ , \\
|\psi_{1/2}^{\Gamma_6^+}(\mathbf{R})\rangle_e &= \frac{1}{\sqrt{2}}\frac{iYZ-XZ}{\mathcal{R}^2}|\mathbf{R},u_{-1/2}^{\Gamma_7}\rangle \ ,
\end{aligned}
\tag{11}
$$

and

$$
|\psi_{1/2}^{\Gamma_6^+}(\mathbf{R})\rangle_f = \frac{1}{\sqrt{2}}\frac{iYZ+XZ}{\mathcal{R}^2}|\mathbf{R},u_{-1/2}^{\Gamma_6}\rangle \ . \tag{12}
$$

X, Y, and Z are the components of $\mathbf{R}$, and $\mathcal{R}^2=|\mathbf{R}|^2=X^2+Y^2+Z^2$. The first entry in Eq. (11) (labeled *a*) is *s*-like, the rest are *d*-like. $|\psi_{1/2}^{\Gamma_6^+}(\mathbf{R})\rangle_f$ in Eq. (12) turns out to be decoupled from the dominant terms *a* and *b* in Eq. (11) and can, as a good approximation, be left out of the basis for the Γ_6^+ states.

Similarly the necessary angular functions for $\Gamma_7^{-1/2}$ acceptor states are found to be

$$
\begin{aligned}
|\psi_{-1/2}^{\Gamma_7^+}(\mathbf{R})\rangle_a &= |\mathbf{R},u_{-1/2}^{\Gamma_7}\rangle \ , \\
|\psi_{-1/2}^{\Gamma_7^+}(\mathbf{R})\rangle_b &= \frac{Z^2-\frac{1}{2}(X^2+Y^2)}{\mathcal{R}^2}|\mathbf{R},u_{-1/2}^{\Gamma_7}\rangle \ , \\
|\psi_{-1/2}^{\Gamma_7^+}(\mathbf{R})\rangle_c &= \frac{\sqrt{3}}{2}\frac{X^2-Y^2}{\mathcal{R}^2}|\mathbf{R},u_{-1/2}^{\Gamma_6}\rangle \ , \\
|\psi_{-1/2}^{\Gamma_7^+}(\mathbf{R})\rangle_d &= \frac{iXY}{\mathcal{R}^2}|\mathbf{R},u_{-1/2}^{\Gamma_6}\rangle \ , \\
|\psi_{-1/2}^{\Gamma_7^+}(\mathbf{R})\rangle_e &= \frac{1}{\sqrt{2}}\frac{iYZ+XZ}{\mathcal{R}^2}|\mathbf{R},u_{1/2}^{\Gamma_6}\rangle \ , \\
|\psi_{-1/2}^{\Gamma_7^+}(\mathbf{R})\rangle_f &= \frac{1}{\sqrt{2}}\frac{iYZ-XZ}{\mathcal{R}^2}|\mathbf{R},u_{1/2}^{\Gamma_7}\rangle \ .
\end{aligned}
\tag{13}
$$

For the Γ_7^+ states the *d*-like contributions are more important, and we keep all angular functions listed in Eq. (13) in the basis.

In the calculations we use a cylindrical cluster of sites on the fcc lattice with the cylinder axis in the *z* direction (the growth direction). The basis functions for the $\Gamma_6^{1/2}$ states ($\Gamma_7^{-1/2}$ states are completely analogous) have the form

$$
|\psi_{1/2}^{\Gamma_6^+}\rangle = \sum_{\mathbf{R}} \cos\left[\frac{\pi}{2}\frac{Z}{Z_{\mathrm{clu}}}\right]\cos\left[\frac{\pi}{2}\frac{(X^2+Y^2)^{1/2}}{R_{\mathrm{clu}}}\right] \times e^{-\alpha(X^2+Y^2+\mu Z^2)^{1/2}}|\psi_{1/2}^{\Gamma_6^+}(\mathbf{R})\rangle \ , \tag{14}
$$

where $2Z_{\mathrm{clu}}$ and R_{clu} are the height and radius of the cylindrical cluster, respectively, and the sum over $\mathbf{R}$ covers all the sites in the cluster except the impurity site. The slowly varying cosine functions are included to avoid a discontinuity in the wave function at the cluster boundary. The α's are chosen to cover a broad range, and for each α we select an appropriate value for the anisotropy parameter μ. The parameter μ allows for compression (or elongation) of the wave function in the *z* direction. Proper values for the α's and μ's are found for each acceptor state separately. For wide quantum wells the acceptor wave functions are qualitatively similar to the exponential functions characteristic for acceptor states in bulk. In narrow wells, where confinement effects are substantial, the wave functions resemble the cosinelike wave functions for pure quantum-well states. For strongly confined states the extension of the cluster in the *z* direction, which affects the shape of the wave function via the cosine factor in Eq. (14), is manually adjusted to obtain the best (i.e., lowest) estimates for the acceptor energies. In addition to seven sets of α's, which give 35 basis functions for Γ_6^+ and 42 basis functions for Γ_7^+, the appropriate bond orbital on the impurity site is included separate-

ly to give a total of 36 and 43 basis functions, respectively.

In order to make the method computationally feasible, we base the algorithm of the computer program on shells, i.e., sites connected by symmetry operations of the point group, instead of single sites. The basis functions of the form in Eq. (14) can equivalently be written as a much smaller sum of shell functions. By considering shell functions instead of single SOBO's when calculating the contents of the matrices in the generalized eigenvalue problem, only one site in each shell has to be included in the double sums. Another crucial simplification follows from the fact that the interaction between two SOBO's does not depend on their absolute positions, only their position relative to each other. Due to this feature, there are a limited number of possible values of interactions between shell functions. In the computer program these interactions are calculated once and stored for reuse. These major simplifications allow for the large cluster sizes required in shallow-acceptor calculations, and up to 630 000 sites for well-centered and 1.9×10^6 sites for barrier-centered acceptors are included in the calculations reported in this article.

C. Scaling approximation

With a maximum of 43 functions in the basis, the *solution* of the generalized eigenvalue problem is a minor task. Even when applying the tricks described above, however, the evaluation of the matrix elements in Eq. (10) generally requires much computer time. To reduce the sizes of the clusters needed in the calculation without substantial loss of accuracy, we use a scaling approximation. The implementation of the approximation in the EBOM method is outlined below (see Ref. 26 for more details).

The effective-mass equation for an acceptor in a single quantum well[13] or superlattice (without any phenomenological short-range potential) has the property that reducing the length scale by a factor s, i.e., $\mathbf{r}'=\mathbf{r}/s$, and making the substitutions

$$Es^2\rightarrow E,\quad \frac{se^2}{\epsilon_0}\rightarrow\frac{e^2}{\epsilon_0},\quad \Delta E_v s^2\rightarrow\Delta E_v\ ,$$
$$L_W/s\rightarrow L_W,\quad L_B/s\rightarrow L_B\ , \tag{15}$$

give an equivalent equation with $\mathbf{r}'$ as independent variable. ΔE_v is the confining well potential due to valence-band offset and L_W and L_B is the well width and barrier width, respectively. Note that the scaling behavior of the spin-orbit coupling is irrelevant since we have assumed the split-off states to be decoupled.

Due to the underlying lattice, this scaling behavior is not an exact property in the EBOM, but may be taken as an approximation. In EBOM calculations for acceptors with a scaling factor $s>1$, a smaller cluster will suffice since the wave function is more localized in space. Given the solution for the scale acceptor problem, the energies (and corresponding wave functions) for the original problem may be determined using the relations in Eq. (15). The approximation is expected to be best for bound states with slowly varying envelopes.

Alternatively, the scaling procedure may be viewed as choosing a larger (and unphysical) lattice constant (sa) and using basis functions consisting of SOBO's located at sites in this coarser lattice in the calculations. From the listing of the interaction parameters in Eq. (4), we see that the interactions between the new SOBO's are inversely proportional to the square of the scaling factor s.

The scaling approximation with $s=2$ is used in most of the calculations of acceptor states in quantum wells and superlattices in the next two sections. For some of the narrowest heterostructures (narrow wells and/or barriers), however, unscaled calculations ($s=1$) are done to achieve a desired higher accuracy.

III. ACCEPTORS IN QUANTUM WELLS

In this section we study C (carbon) and Be (beryllium) acceptors located in the center of the well material in GaAs-$Al_{0.3}Ga_{0.7}As$ single quantum wells. We calculate energies of the Γ_6^+ (heavy-hole) and Γ_7^+ (light-hole) ground states and first even-parity excited states for a wide range of well widths. Energies of the Γ_6 and Γ_7 subband edges, which are required to find estimates for binding energies, are provided by a separate band-structure program within the EBOM formalism. We compare with previous effective-mass calculations and available experimental data. For illustration purposes, we also show some plots of wave functions along high-symmetry directions within the quantum-well plane. At the end of the section we briefly discuss the validity of the choice of boundary conditions at the material interfaces.

The Luttinger parameters and dielectric constants are taken to be

$$\gamma_1=7.65,\quad \gamma_2=2.41,\quad \gamma_3=3.28,\quad \epsilon_0=12.35$$

for GaAs, and

$$\gamma_1=4.04,\quad \gamma_2=0.78,\quad \gamma_3=1.57,\quad \epsilon_0=9.80$$

for AlAs.[34] For the $Al_{0.3}Ga_{0.7}As$ alloy we use a linear interpolation between GaAs and AlAs parameters. The lattice constant a is set to 5.65 Å for both the well and barrier material. The depth of the quantum well is determined by the offset between the valence-band edges E_v, and we use the formula $\Delta E_v=0.35\Delta E_g(x)$,[13] where $\Delta E_g(x)$ is the difference in band gaps at $\mathbf{k}=\mathbf{0}$ between GaAs and $Al_xGa_{1-x}As$. $\Delta E_g(x)$ is taken to be $1247\times x$ meV,[13] with x set to 0.3.

In the calculations of the $1\Gamma_6^+$, $1\Gamma_7^+$, $2\Gamma_6^+$, and $2\Gamma_7^+$ (1 and 2 denote the ground state and first-excited state, respectively), a scaling factor of 2 ($s=2$) is generally used. The only exceptions are for the ground states for the narrowest wells ($L_W<40$ Å), where scaling is not applied. Large cylindrically shaped clusters containing up to 380 000 sites are used in the calculations. The computation for this cluster size takes approximately 3 min on a Cray Research Inc. X-MP/48 (UNICOS) supercomputer for a Γ_6^+ state. U_0 is fitted to make the EBOM predict the right ground state ($1\Gamma_8^+$) energies for the acceptors in bulk GaAs, i.e., in an infinitely wide quantum well.[35] The experimental bulk values are $E_{1\Gamma_8^+}=-26.0$ meV for

C and $E_{1\Gamma_8^+} = -28.0$ meV for Be.[36]

As a check on the validity of the scaling approximation, we calculated the $1\Gamma_6^+$ and $1\Gamma_7^+$ energies for $L_W = 28$ Å, i.e., inside the well-width interval where scaling regularly is not applied, using a scaling factor of 2. Deviations of ~ 0.9 meV for $1\Gamma_6^+$ and ~ 0.6 meV for $1\Gamma_7^+$ were found upon comparison with results obtained from calculations without scaling. The error due to scaling decreases with increasing well width, and for $L_W = 59$ Å we found the differences for the $1\Gamma_6^+$ energies to be reduced to ~ 0.3 meV.

The energies of the $1\Gamma_6^+$, $1\Gamma_7^+$, $2\Gamma_6^+$, and $2\Gamma_7^+$ acceptor states for well widths up to 300 Å are shown in Figs. 1(a) and 1(b) for the C and Be acceptors, respectively. To make comparison with future experiments easier (for not overly narrow wells), we use a smaller energy interval when displaying the Be spectra in Fig. 1(b). The zero of energy is chosen at the bottom of the well, i.e., the GaAs bulk valence-band edge. Since the well width, L_W, is a discrete variable in the EBOM, the results for a set of widths are interpolated to give the curves. Zero well width corresponds to acceptors in the barrier material $Al_{0.3}Ga_{0.7}As$, for which, to our knowledge, no experimental data exist. By assuming the same values of U_0 as for GaAs, binding energies of 33.3 meV for C and 37.7 meV for Be, respectively, are found.[26] These values are used in the extrapolation of the curves to zero well width. From Fig. 1 we see that for well widths larger than ~ 200 Å the ground-state wave functions are essentially unaffected by the presence of the barrier, and both the Γ_6^+ and Γ_7^+ ground states have energies close to the bulk value. The more spatially extended wave functions of the excited states "feel" the barrier, even for the widest wells included in the spectra (300 Å).

In Figs. 1(a) and 1(b) we also plot the Γ_6 and Γ_7 subband edges, which are needed to estimate binding energies. The subband edges are calculated in a separate EBOM program for band structures in quantum wells and superlattices described in detail elsewhere.[24] The Γ_6^+ (Γ_7^+) acceptor binding energy is defined to be the energy difference between the Γ_6 (Γ_7) subband edge and the Γ_6^+ (Γ_7^+) acceptor ground state. Figure 2 shows the Γ_6^+ and Γ_7^+ binding energies for C and Be, respectively, as functions of well width. The curves, with their characteristic single-peak shapes, have maxima for $L_W \sim 12$ Å for Γ_6^+ and $L_W \sim 32$ Å for Γ_7^+. Compared to the analogous calculations for GaAs-$Al_{0.3}Ga_{0.7}As$ spherical quantum dots,[26] the maxima are lower, and this is plausible since the confinement effects are expected to be stronger in heterostructures with confinement in more than one direction. As expected, we find the central-cell shift, i.e., the difference between ground-state energies of Be and C acceptors, to increase due to confinement. The shift is found to be largest for well widths close to the maxima of the binding-energy curves. A shift of up to 5 meV is observed, and this value should be compared with the bulk value of 2 meV.

Our EBOM results are generally in very good agreement with the equivalent effective-mass calculations of Masselink *et al.*[13] for the ground states and binding ener-

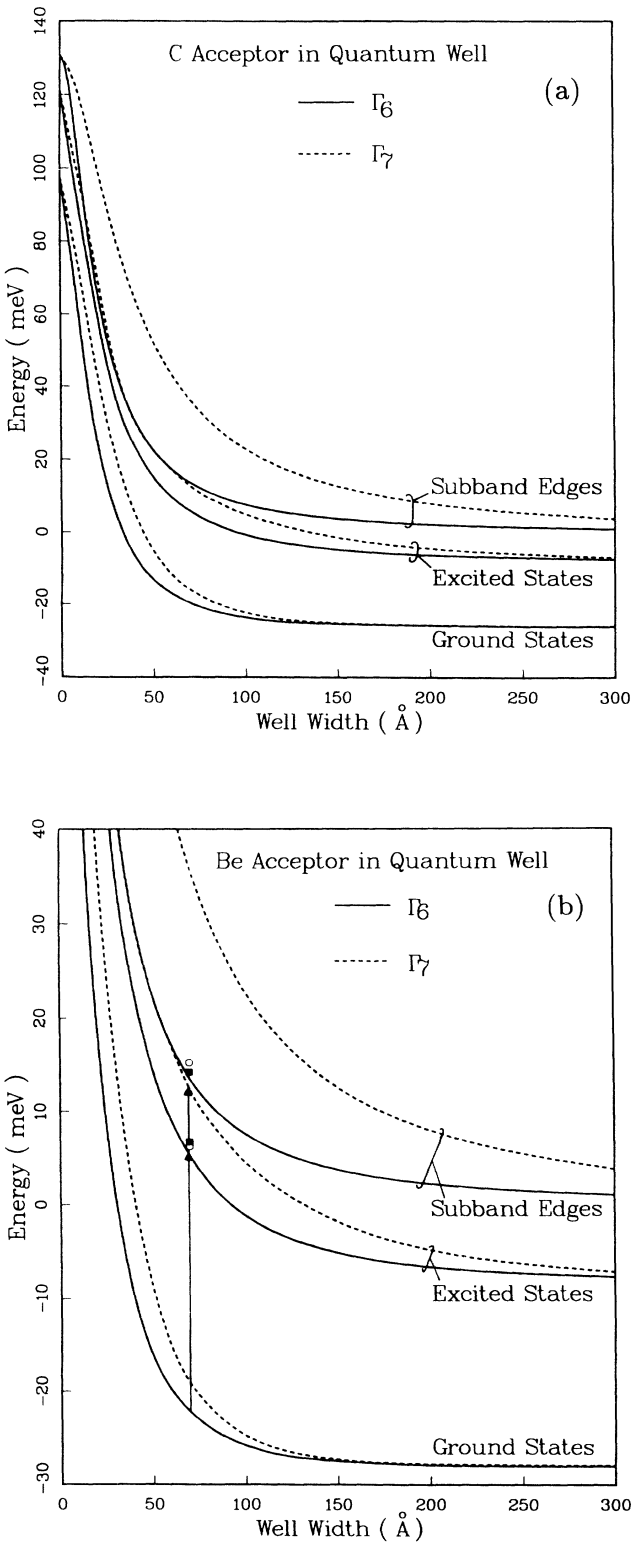

FIG. 1. Energies of the ground states ($1\Gamma_6^+$, $1\Gamma_7^+$), first even-parity excited states ($2\Gamma_6^+$, $2\Gamma_7^+$), and subband edges as functions of well width for (a) C acceptors and (b) Be acceptors centered in GaAs-$Al_{0.3}Ga_{0.7}As$ quantum wells. The valence-band edge of bulk GaAs is chosen as the zero of energy. The arrows in (b) indicate the transitions measured by Holtz *et al.* (Ref. 4). Solid squares represent Raman data, while open circles represent results from two-hole–transition measurements.

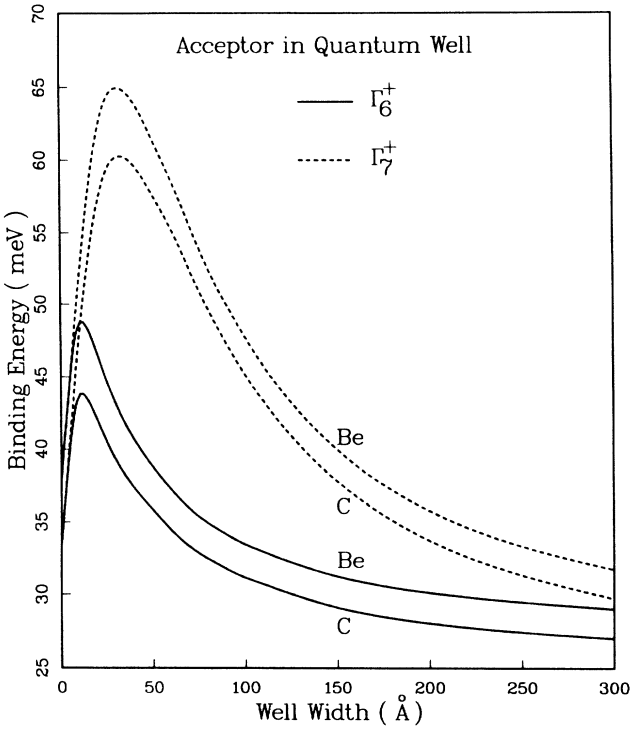

FIG. 2. Binding energies for C and Be acceptors centered in GaAs-$Al_{0.3}Ga_{0.7}As$ quantum wells as functions of well width. The Γ_6^+ (Γ_7^+) binding energy is defined as the energy difference between the Γ_6^+ (Γ_7^+) ground state and the Γ_6 (Γ_7) subband edge.

gies. Small deviations are found when comparing binding energies for the narrowest wells, however, and the EBOM predicts lower maxima in the binding-energy curves compared to effective-mass results. The differences are found to be much larger for the excited states, especially for $2\Gamma_7^+$, and they increase with decreasing well width. While the EBOM estimates for $2\Gamma_6^+$ are typically 3–5 meV lower than corresponding effective-mass results for $L_W < 150$ Å, the EBOM predicts energies 4, 7, and 15 meV lower than effective-mass theory for $2\Gamma_7^+$ for $L_W = 141$, 96, and 51 Å, respectively.

Upon comparison with photoluminescence experiments for Γ_6^+ binding energies, Masselink *et al.* found their results to be in good agreement, and this applies for our EBOM results as well. More recent data from photoluminescence experiments by Liu *et al.*[5] are similarly close to the EBOM (and effective-mass) results.

Although experimental investigation of impurity levels in heterostructures should, in principle, not be more difficult than in bulk, spectra from quantum wells have generally been harder to interpret and predictions of energy levels have often been less accurate. In a recent report, however, Holtz *et al.*[4] applied two different experimental techniques (Raman scattering and selective photoluminescence) to measure energies in Be-doped GaAs-$Al_{0.3}Ga_{0.7}As$ quantum wells 70 Å wide. Two transitions, interpreted as $1\Gamma_6^+$-$2\Gamma_6^+$ and $1\Gamma_6^+$-$2\Gamma_7^+$, were observed in both methods. Raman-scattering measurements gave transition energies of 29.0±0.5 and 36.5±0.5 meV, respectively, while two-hole transitions observed in selective photoluminescence gave 28.5±1 and 37.5±1 meV. EBOM calculations predict slightly lower transition energies, namely 27.6 meV for $1\Gamma_6^+$-$2\Gamma_6^+$ and 34.8 meV for $1\Gamma_6^+$-$2\Gamma_7^+$. We have, for illustrative purposes, indicated the transitions in Fig. 1(b) and marked Raman data by solid squares and two-hole–transition data by open circles. The corresponding results from effective-mass calculations by Masselink *et al.*[13] are given for a so-called ideal acceptor (pure Coulomb impurity potential) with a bulk binding energy of 27.1 meV and must be corrected before comparing with experiments on Be acceptors. By assuming the same central corrections as in the EBOM, transition energies of ~32 meV for $1\Gamma_6^+$-$2\Gamma_6^+$ and ~44–45 meV for $1\Gamma_6^+$-$2\Gamma_7^+$ are obtained. Comparisons with the experimental values favors the EBOM, and we thus generally expect the EBOM estimates for the excited states to be better than the effective-mass results. The deviation in the latter may be due to the following. In this paper we use exponential trial wave functions with different values of μ for different α's, whereas in Ref. 13 Gaussian trial wave functions and a single value of μ for all α's are used. Furthermore, in the present EBOM calculations the extension of the cluster in the z direction is manually adjusted to minimize the acceptor energies for narrow wells. Since the matrix elements in Eq. (10) are not evaluated analytically in the EBOM, there are no practical restrictions on the form or complexity of the trial wave function, in contrast to effective-mass calculations. For the Γ_7^+ states a small fraction of the deviation is due to the absence of the angular function labeled f in Eq. (13) from the basis in the calculations in Ref. 13. In addition, the approximate way of incorporating position-dependent material parameters necessitated by the computational complexity of the effective-mass method may account for part of the difference.

When solving the generalized eigenvalue problem in Eq. (10) to estimate acceptor energies, the wave functions are found as a by-product. The normalization constant has the form

$$\langle \psi | \psi \rangle = \sum_{\mathbf{R}} F(\mathbf{R}) , \tag{16}$$

where $F(\mathbf{R}) = F_{1/2}(\mathbf{R}) = F_{-1/2}(\mathbf{R})$ and the sum covers all sites in the cluster. The quantity $F(\mathbf{R})$ is analogous to the square of the envelope function in effective-mass theory. To illustrate the in-plane anisotropy, i.e., the deviation from cylindrical symmetry, we plot the quantity $|\mathbf{R}_\parallel| F(\mathbf{R}_\parallel, Z=0)$ ($\mathbf{R}_\parallel = [X, Y]$), here called the *in-plane hole density,* for different states of C acceptors centered in quantum wells. The plots are made by interpolating values of the in-plane hole density at points along specific directions, assuming the SOBO's to be nonoverlapping. The validity of the assumption of highly localized SOBO's is uncertain, so care must be taken if the plots are used in quantitative discussions. The in-plane hole density in the [100] and [110] directions for the $1\Gamma_6^+$, $1\Gamma_7^+$, $2\Gamma_6^+$, and $2\Gamma_7^+$ states for a C acceptor centered in a 73-Å-wide quantum well are shown in Figs. 3(a), 3(b),

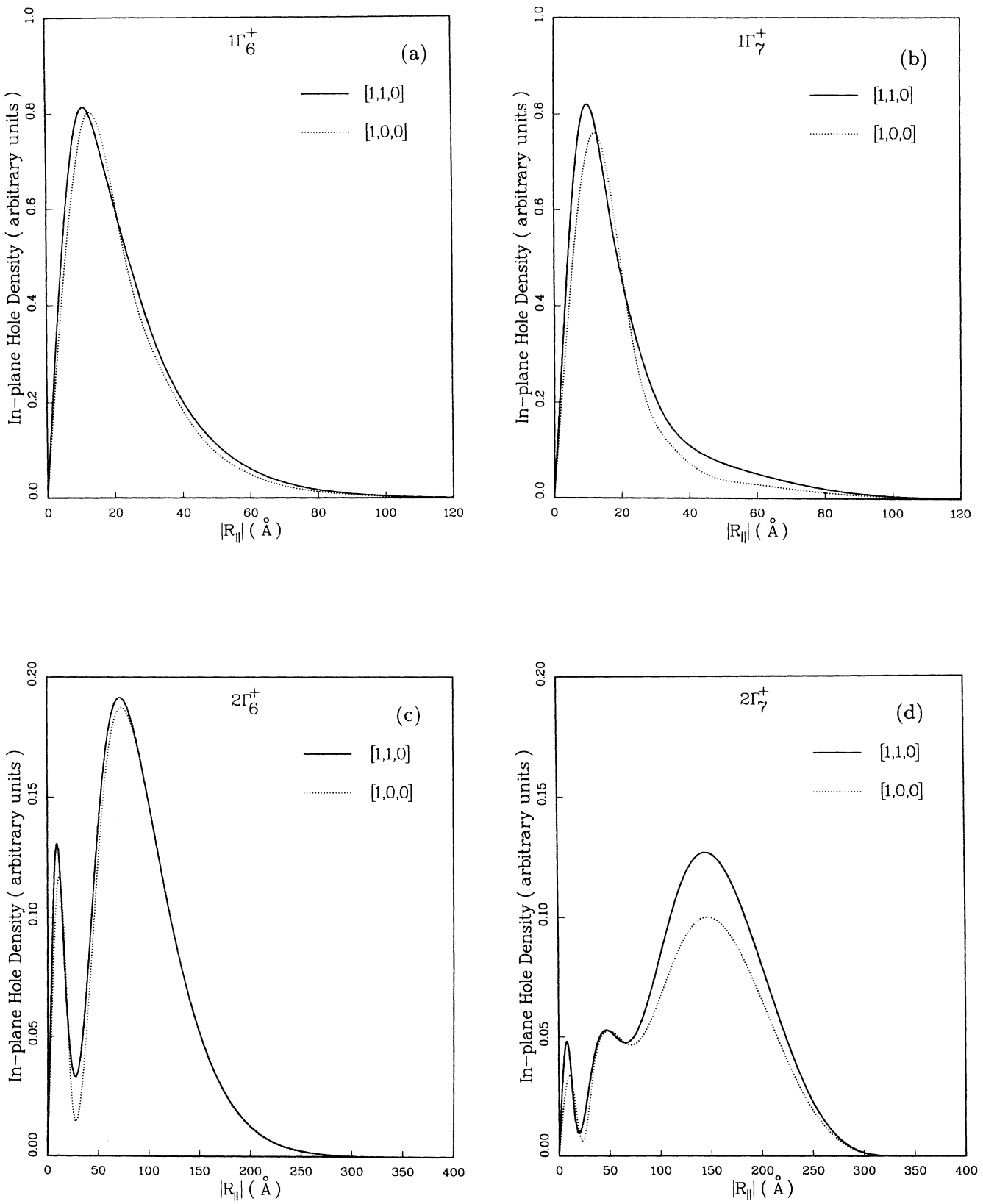

FIG. 3. The in-plane hole density $[|\mathbf{R}_\parallel|F(\mathbf{R}_\parallel, Z=0)]$ in the [100] and [110] directions for (a) the $1\Gamma_6^+$ state, (b) the $1\Gamma_7^+$ state, (c) the $2\Gamma_6^+$ state, and (e) the $2\Gamma_7^+$ state of a C acceptor centered in a 73-Å-wide GaAs-$Al_{0.3}Ga_{0.7}As$ quantum well. The curves are based on calculations with a scaling factor of 2 and are made by interpolating values of the in-plane hole density at points in the given directions.

3(c), and 3(d), respectively. This well width, which arises from scaling with $s=2$ according to Eq. (15), is, strictly speaking, unphysical, but the qualitative behaviors of the corresponding hole densities for similar physical wells (e.g., $L_W=71$ or 76 Å) are expected to be the same. A notable feature is the stronger anisotropy of the Γ_7^+ wave functions compared to Γ_6^+. The anisotropy, which reflects the importance of d-like contributions is strongest for the Γ_7^+ excited state. Note, also, the larger spatial extension of the wave function of the $2\Gamma_7^+$ state compared to $2\Gamma_6^+$. For the ground states we find the hole, on the average, to be closer to the acceptor than for a C acceptor in bulk ($\langle|\mathbf{R}|\rangle \sim 31$ and ~ 29 Å for $1\Gamma_6^+$ and $1\Gamma_7^+$, respectively, compared to ~ 36 Å for bulk[26]). When comparing the excited states with the corresponding $2\Gamma_8^+$ bulk state ($\langle|\mathbf{R}|\rangle \sim 107$ Å), we find the hole, on the average, to be closer for $2\Gamma_6^+$ but farther away for the $2\Gamma_7^+$ state.

To check the sensitivity to the choice of boundary conditions, we calculated, without scaling, the Γ_6^+ ground-state energy for a C acceptor in a 59-Å-wide quantum well using a set of different boundary conditions. With pure GaAs parameters for the interactions across the boundary, the ground-state energy is lowered by 13 meV when compared to the average-boundary-condition value of -17 meV. Similarly, this energy is raised by 5 meV when pure $Al_{0.3}Ga_{0.7}As$ parameters are used. The good agreement found earlier in this section when comparing EBOM results with experiments indicates that the average boundary conditions probably are close to the right boundary conditions for high-quality quantum-well or superlattice interfaces.

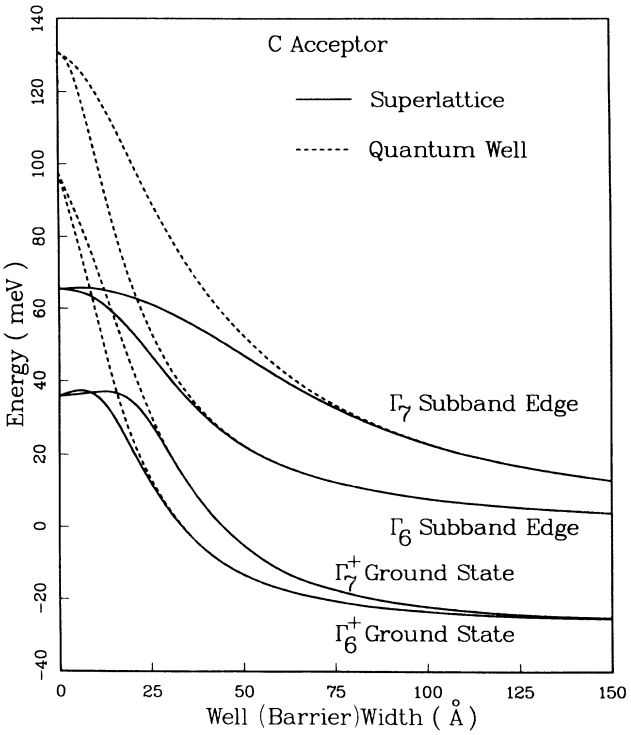

FIG. 4. Energies of the ground states ($1\Gamma_6^+, 1\Gamma_7^+$) for C acceptors centered in the well material of GaAs-$Al_{0.3}Ga_{0.7}As$ single quantum wells and superlattices, respectively, as functions of well width. The Γ_6 and Γ_7 subband edges are also shown. For the superlattices the well widths and barrier widths are equal. The valence-band edge of bulk GaAs is chosen as the zero of energy.

IV. ACCEPTORS IN SUPERLATTICES

In this section we first study acceptors in superlattices incorporating several wells in the model. The effect of the coupling of adjacent wells is studied and the calculated energy spectra are discussed and compared with results from similar donor calculations within the effective-mass framework. Finally, EBOM calculations are compared with data from recent measurements on a set of samples where acceptors are embedded in both well and barrier material, and the barriers are sufficiently thin to make coupling of adjacent wells important.

First, we focus on C and Be acceptors centered in the well material of GaAs-$Al_{0.3}Ga_{0.7}As$ superlattices with equal well and barrier widths ($L_W=L_B=L$). We calculate the energies of the Γ_6^+ and Γ_7^+ ground states using the same material parameters as in Sec. III. As in the quantum-well calculations, a scaling factor of 2 is used for $L_W>40$ Å. Coupling between adjacent wells increases as the well and barrier widths decrease, and up to 11 wells are included in the calculations on the superlattices with the shortest periods. To calculate the Γ_6^+ and Γ_7^+ binding energies, the Γ_6 and Γ_7 subband edges are needed, and, as for the single quantum wells, they are provided by a separate EBOM program.

Figure 4 shows the Γ_6^+ and Γ_7^+ ground-state energies for a C acceptor and corresponding subband edges as functions of the thickness of the well (or barrier). In the extrapolation to zero thickness for the ground-state energies, we use the average of the energies for the acceptor in bulk GaAs and $Al_{0.3}Ga_{0.7}As$. For the zero-thickness value for the subband-edge energies, we use half the value of the valence-band offset, i.e., the offset between GaAs and $Al_{0.15}Ga_{0.85}As$. The corresponding energy spectra for a single quantum well are shown with dashed lines to illustrate the importance of coupling of adjacent wells. The interwell coupling is strongest for the Γ_7 states. Since the acceptor confines the hole to the vicinity of the impurity, we expect the interwell coupling to be relatively less important for acceptor states compared to the extended Bloch states corresponding to the subband edges. This is indeed observed. For the acceptor ground states, we see from Fig. 4 that the wells are essentially decoupled, i.e., there is no difference between energies for the superlattice and quantum well, for widths larger than ~ 30 Å. For the Γ_7 subband energy, however, the effect of coupling is seen in superlattices with well (or barrier) widths up to 75 Å.

The corresponding Γ_6^+ and Γ_7^+ binding energies for C and Be acceptors are shown in Figs. 5(a) and 5(b), respectively. For comparison, we show with dashed lines the binding-energy spectra for the same acceptors centered in a single quantum well. The maxima in the superlattice spectra are seen to be lower and shifted towards higher

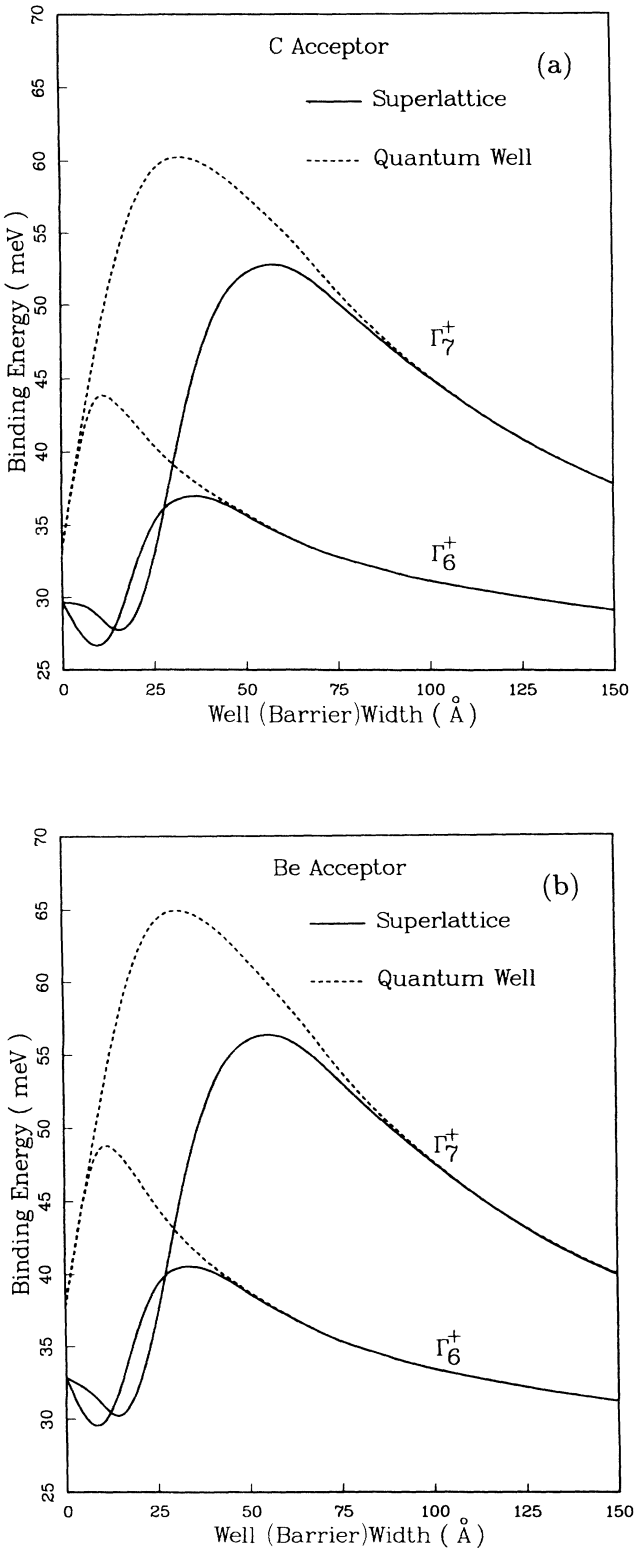

FIG. 5. Binding energies for (a) C acceptors and (b) Be acceptors centered in the well material of GaAs-$Al_{0.3}Ga_{0.7}As$ single quantum wells and superlattices, respectively, as functions of well width. For the superlattices the well widths and barrier widths are equal. The Γ_6^+ (Γ_7^+) binding energy is defined as the energy difference between the Γ_6^+ (Γ_7^+) ground state and the Γ_6 (Γ_7) subband edge.

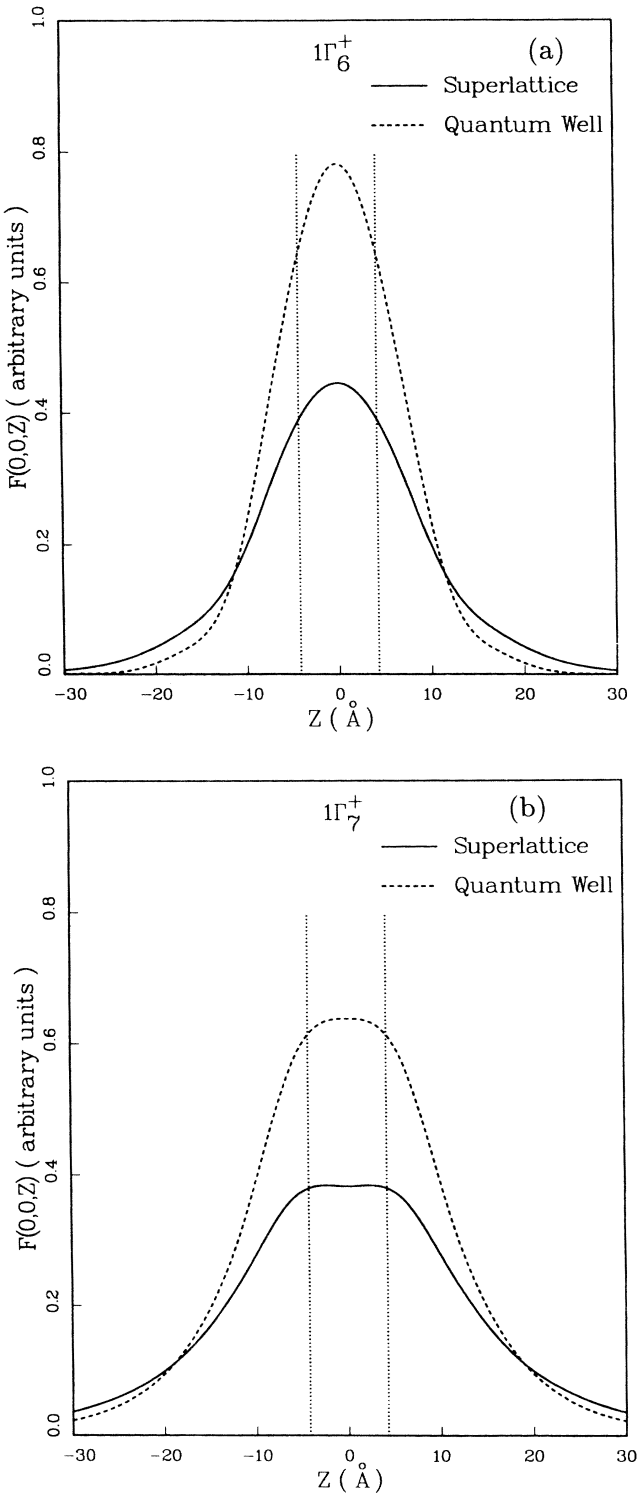

FIG. 6. $F(\mathbf{R})$, defined in Eq. (16), in the [001] direction for (a) the $1\Gamma_6^+$ states and (b) the $1\Gamma_7^+$ states of a C acceptor centered in the well material of an 8.5-Å-wide single quantum well and a superlattice with well and barrier widths of 8.5 Å, respectively. $F(\mathbf{R})$ is analogous to the square of the envelope function in effective-mass theory. The vertical dotted lines represent the interfaces between the well and barrier in the quantum well (and also the interfaces closest to the acceptor impurity in the superlattice). The plots are made by interpolating calculated values of $F(\mathbf{R})$ at points on the z axis.

TABLE I. Γ_6^+ (heavy-hole) binding energies for C acceptors centered in the well material in GaAs-$Al_xGa_{1-x}As$ superlattices. x is alloy composition, L_W is well width, L_β is barrier width, E_W is the Γ_6^+ binding energy for well-centered acceptors, and $E_{X_{hh}}$ is the estimated binding energy for heavy-hole (Γ_6) excitons. The experimental values of E_W are found by adding the estimated values of $E_{X_{hh}}$ to the measured values of $E_W - E_{X_{hh}}$. All samples are grown by MOCVD, except sample 3, which is grown by MBE. For samples 1–4 the listed EBOM results are found by linear interpolation between values for E_W from calculations with $L_W = 76$ and 82 Å. All energies are in meV, and all widths are in Å.

Sample no.	x	L_W	L_B	$E_W - E_{X_{hh}}$ Expt.	$E_{X_{hh}}$	E_W Expt.	E_W EBOM
1	0.1	80	20	26.8	4.1	30.9	29.9
2	0.3	80	20	27.1	4.5	31.6	31.7
3	0.3	80	20	27.9	4.5	32.4	31.7
4	0.5	80	20	25.8	5.1	30.9	31.9
5	0.3	180	20	23.8	5.2	29.0	28.4
6	0.3	280	20	20.8	5.1	25.9	27.2

well widths. When comparing with Chaudhuri's (single-band) effective-mass donor calculations,[14] we find the same qualitative behavior, except for the thinnest structures. As expected, the sharp maximum for small widths, which is found in the donor calculations involving only three wells, is nonexistent in our extended model involving 11 wells.

To further illustrate the coupling of wells, we plot the quantity $F(\mathbf{R})$, as defined in Eq. (16), along the z axis (growth direction) for the ground states of a C acceptor centered in the well material of a superlattice with $L_W = L_B = 8.5$ Å and a single quantum well with the same well width, respectively. $F(0,0,Z)$ for the Γ_6^+ and Γ_7^+ ground states are shown in Figs. 6(a) and 6(b). As in Sec. III, discrete values of $F(\mathbf{R})$, assuming pointlike SOBO's, are interpolated to give the smooth curves shown in Fig. 6. The superlattice wave functions are observed to be more extended in the z direction than the quantum-well wave functions, due to interwell coupling. Note, also, the larger extension in the z direction of the Γ_7^+ wave functions compared to Γ_6^+.

Recently, Skromme *et al.* made photoluminescence measurements on a series of superlattice samples, predominantly MOCVD grown, with thin barriers.[3,27] Peaks interpreted as transitions involving bound states of residual C acceptors centered in the well and barrier material, respectively, were observed in the spectra. We have performed calculations of binding energies for well- and barrier-centered C acceptors in these superlattices. The parameters describing the superlattices in the calculations are naturally chosen according to the composition of the samples used in the measurements. In the experiments the difference between the Γ_6^+ acceptor binding energy and the binding energy of Γ_6 (heavy-hole) excitons is measured, and estimates of the binding energies of these excitons are thus needed to facilitate comparison with the EBOM results. These estimates are found using the **k**-space–sampling method, introduced by Chu and Chang, on an axial effective-mass model including only one conduction subband and one valence subband.[37] The resulting exciton binding energies are listed in Table I (and II). Due to the neglect of coupling to other subbands, we expect the predicted values for the exciton binding energies to be slightly too low. The deviation is presumably largest for the samples with the widest wells, where separate subbands are energetically close.

In the calculations for acceptors located in the barrier material, we assume the same value of U_0 as in the well material. For most of the superlattices used in the measurements, the EBOM results are insensitive to (reasonable) variations in U_0, so the correctness of the choice of this parameter is generally not important for barrier-centered acceptors. The only exception is sample 1 in Table I (and II), where the central-cell shift is roughly

TABLE II. Same as Table I for C acceptors centered in the barrier material in GaAs-$Al_xGa_{1-x}As$ superlattices. E_B is the Γ_6^+ binding energy for barrier-centered acceptors.

Sample no.	x	L_W	L_B	$E_B - E_{X_{hh}}$ Expt.	$E_{X_{hh}}$	E_B Expt.	E_B EBOM
1	0.1	80	20	9.5	4.1	13.6	17.4
2	0.3	80	20	8.7	4.5	13.2	11.2
3	0.3	80	20	8.3	4.5	12.8	11.2
4	0.5	80	20	2.9	5.1	8.0	10.1
5	0.3	180	20	4.2	5.2	9.4	8.2
6	0.3	280	20	0.4	5.1	5.5	7.1

half of the corresponding bulk value.

The scaling approximation is not used in the calculations. Larger clusters are generally needed in EBOM calculations for acceptors centered in the barrier than for acceptors centered in the well. The maximum number of sites included in these calculations is 1.9×10^6 sites for barrier-centered and 630 000 for well-centered acceptors. For well-centered acceptors in samples 5 and 6, the confinement effects are minimal, and the single-quantum-well results in the preceding section apply.

For the valence-band offset we use the same formula as in Sec. III for the alloys $x=0.1$, 0.3, and 0.5, i.e., $\Delta E_v=0.35\times1247\times x$ meV, although this formula, strictly speaking, is only recommended for $x<0.45$.[34]

The experimental data and the corresponding EBOM results for the Γ_6^+ binding energies for well- and barrier-centered acceptors are listed in Tables I and II, respectively. The agreement is found to be quite good for the well-centered acceptors, where the deviations are less than 1.5 meV for all samples. The agreement for the barrier-centered acceptors is not as good. Deviations are typically 1–2 meV, with the exception of sample 1, where a deviation of 3.8 meV is observed. However, it is known that due to the growth technique employed, the actual sample parameters differed significantly from the nominal values listed in the tables.[38] This may affect the comparison of EBOM results and the experimental data. Additional experiments are in progress to measure more accurately the actual sample parameters to permit a better comparison with theory.[27]

VI. CONCLUDING REMARKS

We have studied acceptors in quantum wells and superlattices using the effective bond-orbital model (EBOM).[24,26] The agreement with available experimental data is generally good.

The EBOM method has several advantages in acceptor calculations as compared to the effective-mass theory: the positional dependence of the material parameters is straightforward to incorporate in the calculations, more flexible trial wave functions can be used in the variational calculations, and more complicated heterostructures (e.g., several coupled quantum wells) can be handled. For acceptors centered in single quantum wells, the results from the EBOM are in good agreement with previous effective-mass results (and available experimental data) for the Γ_6^+ and Γ_7^+ ground states, but the results for the energies of the first even-parity excited states differ. Comparisons with recent experiments, where two separate experimental techniques are used to measure transition energies involving these excited states, favor the EBOM results. The discrepancies between the effective-mass results are presumably mainly due to the first and/or second shortcoming mentioned above. In the calculations on acceptors in superlattices with thin barriers and wells, we were able to include 11 wells in the model without calculational difficulties. The inclusion of only three wells in the analogous effective-mass calculations for donors was partly due to the calculational complications of incorporating more wells in the model.

Since the EBOM assumes no lattice defects and perfect interfaces, we expect the results to be in closest agreement with measurements on high-quality samples. When the EBOM is applicable, we also expect the appropriate boundary conditions to be close to the average boundary condition used in this article.

ACKNOWLEDGMENTS

We would like to thank B. J. Skromme for useful discussions and for providing us with experimental data prior to publication. H. Chu provided the computer code for the exciton calculations and is acknowledged. Fruitful discussions with A. Cancio and D. S. Citrin are also acknowledged. One of us (G.T.E.) would like to thank the group of Y.-C. Chang for the hospitality shown during his visit. He would also like to thank United States Educational Foundation in Norway (Fulbright) and the Royal Norwegian Council for Scientific and Industrial Research (NTNF) for financial support during the stay at the University of Illinois at Urbana-Champaign (UIUC). This work was supported in part by the U.S. Office of Naval Research (ONR) under Contract No. N00014-89-J-1157. We acknowledge the use of the Cray Research, Inc., X-MP/48 supercomputer at the National Center for Supercomputer Applications at UIUC.

[1]B. V. Shanabrook and J. Comas, Surf. Sci. **142**, 504 (1984).

[2]R. C. Miller, A. C. Gossard, W. T. Tsang, and O. Munteanu, Phys. Rev. B **25**, 3871 (1982).

[3]B. J. Skromme, R. Bhat, and M. A. Koza, Solid State Commun. **66**, 543 (1988).

[4]P. O. Holtz, M. Sundaram, R. Simes, J. L. Merz, A. C. Gossard, and J. H. English, Phys. Rev. B **39**, 13 293 (1989).

[5]X. Liu, A. Petrou, A. L. Moretti, F. A. Chambers, and G. P. Devane, Superlatt. Microstruct. **4**, 141 (1988).

[6]B. V. Shanabrook, J. Comas, T. A. Perry, and R. Merlin, Phys. Rev. B **29**, 7096 (1984).

[7]D. Gammon, R. Merlin, W. T. Masselink, and H. Morkoç, Phys. Rev. B **33**, 2919 (1986).

[8]N. C. Jarosik, B. D. McCombe, B. V. Shanabrook, J. Comas, R. J. Wagner, and G. Wicks, in *Proceedings of the 17th International Conference on the Physics of Semiconductors, San Francisco, 1984,* edited by J. D. Chadi and W. A. Harrison (Springer, New York, 1985).

[9]A. A. Reeder, B. D. McCombe, F. A. Chambers, and G. P. Devane, Phys. Rev. B **38**, 4318 (1988).

[10]G. Bastard, Phys. Rev. B **24**, 4714 (1981).

[11]C. Mailhiot, Y.-C. Chang, and T. C. McGill, Phys. Rev. B **26**, 4449 (1982).

[12]R. L. Greene and K. K. Bajaj, Solid State Commun. **45**, 825

(1983).
[13]W. T. Masselink, Y.-C. Chang, and H. Morkoç, Phys. Rev. B **32**, 5190 (1985).
[14]S. Chaudhuri, Phys. Rev. B **28**, 4480 (1983).
[15]J. M. Luttinger and W. Kohn, Phys. Rev. **97**, 869 (1955).
[16]G. T. Einevoll and P. C. Hemmer, J. Phys. C **21**, L1193 (1988).
[17]D. J. BenDaniel and C. B. Duke, Phys. Rev. **152**, 683 (1966).
[18]G. Bastard, Phys. Rev. B **24**, 5693 (1981).
[19]J. Thomsen, G. T. Einevoll, and P. C. Hemmer, Phys. Rev. B **39**, 12 783 (1989).
[20]I. Galbraith and G. Duggan, Phys. Rev. B **38**, 10 057 (1988).
[21]K. Young, Phys. Rev. B **39**, 13 434 (1989).
[22]See, e.g., M. Altarelli, in *Interfaces, Quantum Wells, and Superlattices,* No. 179 of *NATO Advanced Study Institute Series, Series B: Physics,* edited by C. R. Leavens and R. Taylor (Plenum, New York, 1988).
[23]W. A. Harrison, Phys. Rev. B **8**, 4487 (1973).
[24]Y.-C. Chang, Phys. Rev. B **37**, 8215 (1988).
[25]M.-P. Houng and Y.-C. Chang, J. Appl. Phys. **64**, 4609 (1988); **65**, 3092 (1989).
[26]G. T. Einevoll and Y.-C. Chang, Phys. Rev. B **40**, 9683 (1989).
[27]B. J. Skromme, R. Bhat, and M. A. Koza (unpublished).
[28]J. C. Slater and G. F. Koster, Phys. Rev. **94**, 1498 (1954).
[29]J. M. Luttinger, Phys. Rev. **102**, 1030 (1956).
[30]L. Oliveira, Phys. Rev. B **38**, 10 641 (1988).
[31]A recent report [D. D. Coon and H. C. Liu, Superlatt. Microstruct. **3**, 95 (1987)] indicates that this approximation is good for impurities in quantum wells.
[32]G. F. Koster, J. O. Dimmock, R. G. Wheeler, and H. Statz, *Properties of the Thirty-Two Point Groups* (MIT Press, Cambridge, MA, 1963).
[33]F. C. Von der Lage and H. A. Bethe, Phys. Rev. **71**, 612 (1947).
[34]As compiled by J. C. M. Henning, J. J. P. Noijen, and A. G. M. denNijs, Phys. Rev. B **27**, 7451 (1983).
[35]Since we use a different set of basis functions here than in the bulk and quantum-dot calculations in Ref. 26, the fitted values of U_0 are not exactly the same.
[36]D. J. Ashen, P. J. Dean, D. T. J. Hurle, J. B. Mullin, A. M. White, and P. D. Greene, J. Phys. Chem. Solids **36**, 1041 (1975).
[37]The computer program is a smaller version of the program used in H. Chu and Y.-C. Chang, Phys. Rev. B **39**, 10 861 (1989).
[38]B. J. Skromme (private communication).